The Effect of ZnO Growth Temperature on the Memristive Behaviour of Hybrid ZnO-Graphene Thin Film

Tengku Norazman Tengku Abd Aziz, Aimi Bazilah Rosli, Marmeezee Mohd Yusoff, Sukreen Hana Herman, Zurita Zulkifli

Abstract— **Hybrid ZnO-Graphene devices have revealed a stable switching cycle compared to ZnO devices. They have better memristive performance and are suitable in non-volatile memory applications. Here, we report the effect of ZnO growth temperature on the memristive effect of ZnO and hybrid ZnO-Graphene thin films. We show the electrical, optical and morphological properties of the devices using Thermal Chemical Vapour Deposition (TCVD) and Water Bath methods. The relationship between ZnO morphological structure and carrier mobility is discussed. Additionally, the effect of Graphene insertion is shown in the number of switching cycles. It was found that the ZnO thin film deposited at 350°C showed high resistance ratio of about 3.17 due to the defects present in the crystal structure. On the other hand, nanoparticles in 450°C and 550°C samples resulted in thicker films that reduced the memristive window to 1.9 and 2.6 respectively. Hybrid devices exhibited increased stability at switching cycle 4 compared to ZnO devices.**

Keywords— *Graphene, TCVD, Water Bath, ZnO*

I. INTRODUCTION

New era of computing that demands miniaturization of devices and improvement of performance has led to the effort in the semiconductor industry to focus on the development of nanoscale structures. In this regard, memristors development is fitting with this framework whereby memristive devices are highly scalable to the tune of nanometer scale [1]. They have great potentials in applications such as non-volatile memory and resistive switching devices.

There are many materials that are suitable for this purpose. Among them are perovskite oxide materials [2], binary transition metal oxides (like ZnO [3], TiO2 [4], Ta2O5 [5], NiO [6]), chalcogenides [7], organic materials [8], [9] and carbon-based devices, specifically those based on Graphene and Graphene Oxide [10].

However, many of the devices have drawbacks in terms of endurance and set/reset variability. By combining metal oxide such as ZnO with Graphene, the hybrid device can exhibit longer lasting memristive devices [11]. For example, the insertion of Graphene blocks atomic diffusion, altering the oxygen vacancy interactions between metal and insulator [12]. In another study, the integration of large-area CVD Graphene into titanate-based memristive devices has reduced switching power and nonlinear I-V characteristics while maintaining the device performance [13].

In this work, we combined TCVD ZnO at various growth temperatures with Graphene to understand the effect of the device memristive behaviour. We investigated the changes in the morphological structures of ZnO that contributed to the enhancement of hysteresis window. In addition, the stability of the device was improved when Graphene was inserted into the ZnO thin film.

II. EXPERIMENTAL DETAILS

A. Thin film preparation

A microscope glass slide cut into 2x2 cm² was used as a substrate for the Pt deposition. A 60 nm thick of Pt was deposited using electron beam evaporation. Then, a thin layer of about 30 nm of stabilizing Pt was deposited using physical vapour sputtering to allow for the stability of hysteresis loop.

The active material consisting of ZnO was deposited on the substrate using TCVD with the growth temperature that was varied from 350°C to 550°C with 100°C interval. The ZnO thin film was synthesized from the precursor in Zn powder (99.9% purity; Sigma-Aldrich). The parameters that were fixed included the precursor temperature at 750°C, Argon gas flow rate at 69 sccm, Oxygen flow rate at 5 sccm, deposition time for 1 hr and precursor weight at 500 mg.

The sample was then placed into a furnace for annealing for 1 hr at 500°C to improve the crystallinity of the ZnO thin film and to make the Pt layer adhere firmly to the substrate.

After the annealing, the sample was deposited with Graphene using water bath. The source of Graphene was 0.4-0.5 wt% Graphene in water solution (purchased from Nanstructured & Amorphous Materials Inc.). 1 ml of Graphene mixture was added to 18 ml deionized (DI) water. The resulting mixture was added into Schott bottle and sonicated for about 1.5 minutes to allow Graphene to disperse well in the mixture. Then the substrate was placed into the bottle with the Pt surface facing upwards. The substrate was immersed in the water bath at 90°C for 3 hrs. The parameters of the water bath included 3 hrs for the water bath time, 90°C for the bath temperature, 1 ml for the liquid graphene

concentration, 18 ml for the DI water concentration, and 1.5 mins for the sonication time.

B. Characterization

Platinum (Pt) was used as the metal contact, which was deposited using Electron Beam Evaporation (EBE) at the base of the device to form the Bottom Electrode (BE) and at the top surface of the device to form the Top Electrode (TE). A metal mask was used to make the TE. Characterizations were carried out on the device using Field Emission Scanning Electron Microscope (FESEM) (JEOL JSM-7600F) (operating voltage between 0.02 and 30 kV) to analyse the ZnO morphology, UV-vis (Jasco V-670) to learn about both the ZnO and ZnO-Graphene device transmittance, Raman spectroscopy (Horiba LabRam HR Evolution) (514 nm laser) to determine the presence of Graphene in the hybrid ZnO-Graphene thin film and Current-Voltage (IV) measurements (Keysight B1500A Semiconductor Device Parameter Analyzer) to understand the memristive behaviour of the samples.

III.   RESULTS AND DISCUSSION

A. Morphological Structure

Figure **1** shows the morphology of the samples using FESEM at 50KX. It can be seen that all ZnO samples prepared at 350°C, 450°C and 550°C have uniform morphology. However, there is a difference in the morphological structure of each sample in terms of the grain size. The largest grain size can be seen in the 450°C, where the grain boundary coalesces with each other to form larger 3D islands. These grains are large enough to cover voids and pores located on the surface of the sample, forming dense films.

On the other hand, smaller grains seen in 350°C ZnO sample can cause higher electrical resistance because electrons have less continuous paths between adjacent grains. Thus, it takes longer for the electrons to travel within the crystal lattice.

Higher temperature gives rise to the grains that coalesce into flat and dense surface morphology [14]. The 3D islands are more pronounced because the density of nucleation sites is higher in 450°C sample. As the thin film becomes thicker, secondary nucleation grows on the sides of the ZnO islands, causing anisotropic growth [15]. The growth extends further to form secondary nucleation sites, which develop into the base for 2D nanoparticle growth. The nanoparticles further grow into nanorods in 450°C and 550°C samples, increasing the samples conductivity.

Figure 2 shows Graphene deposited on ZnO at 350°C, 450°C and 550°C. It can be seen that Graphene covers the ZnO thin film, forming a continuous layer.
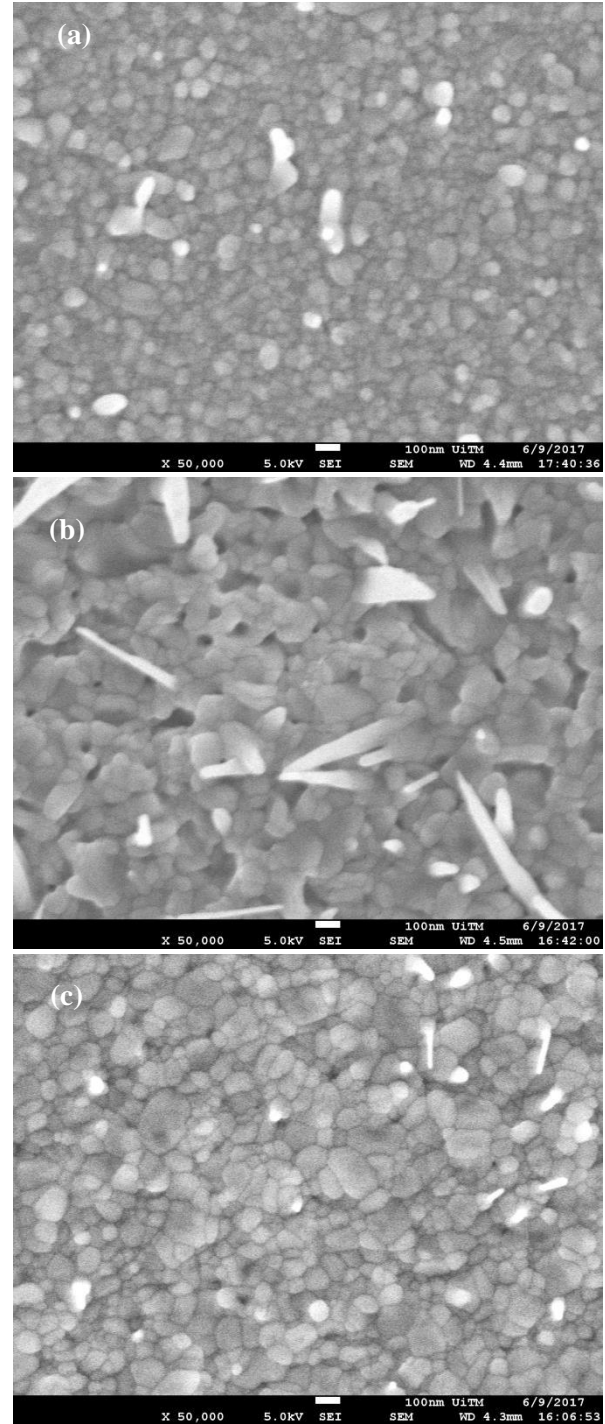
Figure 1 shows the FESEM images of ZnO deposited at temperatures of (a) 350°C (b) 450°C (c) 550°C
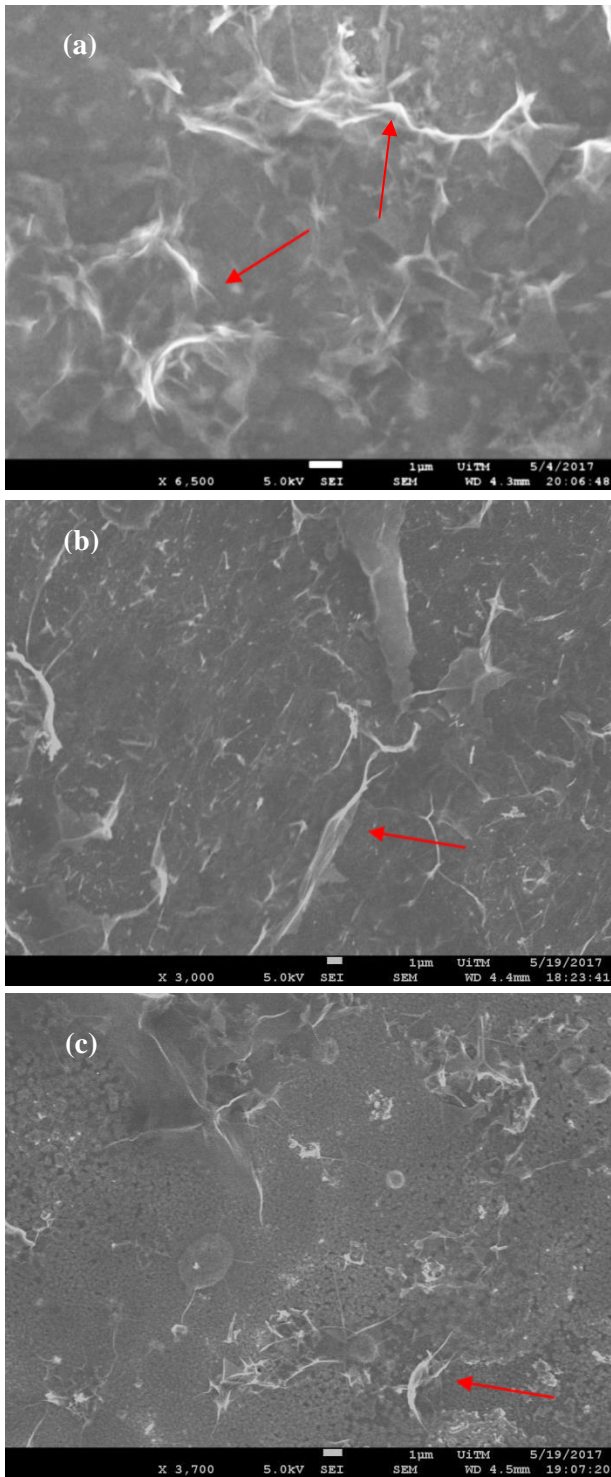
Figure 2 shows the FESEM images of Graphene (folded graphene-red arrow) on ZnO deposited at temperatures of (a) 350˚C (b) 450˚C and (c) 550˚C

B. Raman Spectra

Figure 3(a)-(c) show the Raman spectra of ZnO-Graphene thin film on glass substrate for 350˚C, 450˚C and 550˚C. It can be confirmed from Figure 3 that Graphene is present in all samples. The D bands are at 1346 cm^{-1}, 1344 cm^{-1} and 1348 cm^{-1} for samples prepared at 350˚C, 450˚C and 550˚C respectively, whereas the G bands are at 1580.7 cm^{-1}, 1587.4 cm^{-1} and 1584.1 cm^{-1} respectively.

The high D band peak suggests the presence of defect, such as the disruption of sp^2 bonding, on the graphene surface. This may be attributed to the sonication process that damages the layer. Another disorder of the graphene layer is the weak 2D intensity at 2671 cm^{-1}, 2737 cm^{-1} and 2670 cm^{-1} for samples at 350˚C, 450˚C and 550˚C respectively. The low 2D peak is associated with the presence of a multilayered graphene. The random disorder and the shape evolution make the unique assignment of the 2D peak very difficult. It has been shown in the past that the high D band and low 2D band is a characteristic of multilayered graphene [16]. The intensity effects seen in D and 2D bands may be due to the water bath process that exposes the surface to water molecules, which in turn oxidize the surface.

In Figure 3(b), two sharp peaks of ZnO at 431.2 cm^{-1} and 562.9 cm^{-1} can be seen in 450˚C sample. The peaks correspond to E_2 mode and A_1 mode respectively. At 550˚C in Figure 3(c), both peaks, which are lower than at 450˚C, can be seen at 431.2 cm^{-1} and 570.5 cm^{-1} respectively. The lowest peaks for ZnO can be seen in Figure 3(a), where the growth temperature is 350˚C. The peaks are at 433 cm^{-1} and 568.6 cm^{-1} respectively.
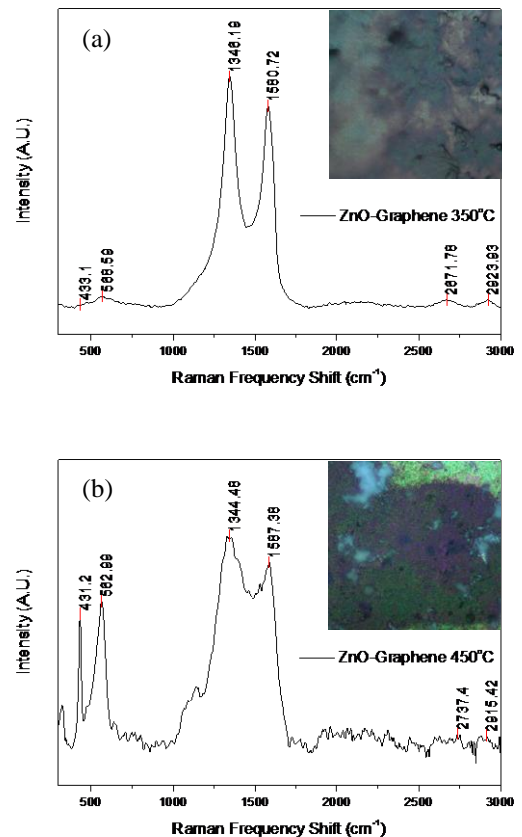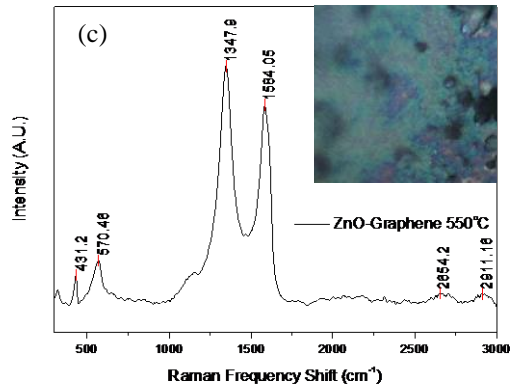
Figure 3 (a)-(c) show the Raman spectra of the ZnO-Graphene samples at different deposition temperature. The insets show the 100X optical microscopy image of the laser spot for each sample

Figure 4 shows the comparison of D and G peaks of ZnO-Graphene at 350°C, 450°C and 550°C. To analyse the defects of Graphene after the its deposition on ZnO, the ratio of I_D/I_G is calculated. The ratio is a measure of sp^2/sp^3 carbon ratio, which signifies the disorder in Graphene [17]. The decrease in the ratio value implies the increase in sp^2 domains, which in turn suggests the extent of oxidation to the Graphene carbon ring [18].
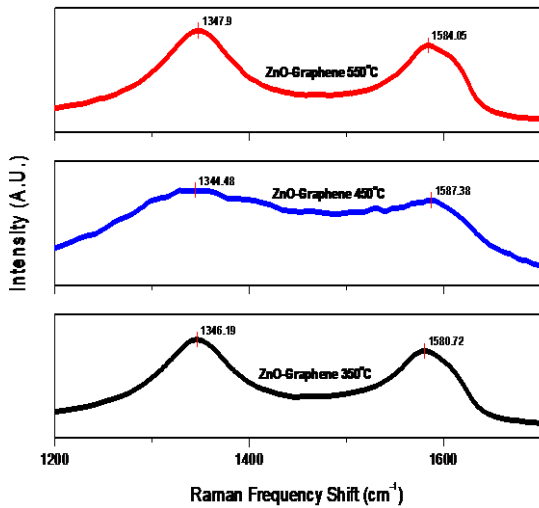
Figure 4 D and G bands for ZnO-Graphene samples at 350°C, 450°C and 550°C

The calculation of I_D/I_G ratio is based on either the peak area of D and G for small defect or the intensity of D and G for large defect. Since the D peak is sharp and intense in the case of ZnO-Graphene samples, the calculation is based on the peak intensity of D and G. From the calculation, the ratios for ZnO-Graphene at 350°C, 450°C and 550°C are 1.2, 1.14 and 1.15 respectively.

TABLE I. I_D/I_G RATIO FOR ZNO-GRAPHENE SAMPLES

ZnO growth temperature	I_D/I_G ratio
350°C	1.15
450°C	1.14
550°C	1.2

From table 1, it can be seen that the I_D/I_G ratio increases as the growth temperature is decreased. At low temperature, the grain size is small as seen in Figure 1. This leads to ZnO crystallinity that contains higher number of defects in the form of oxygen vacancies. As seen in Figure 5, the ZnO peak at 433.1 cm^{-1} for 350°C sample is low compared to 450°C and 550°C samples. The low peak implies that the degree of crystallinity is low. This also means that 350°C ZnO sample contains more oxygen vacancies and oxygen ions that can form bonding with Graphene through C-O-Zn [19]. The bonding oxidizes Graphene and reduces the sp^2 domains. As a result, Graphene disorder is increased.
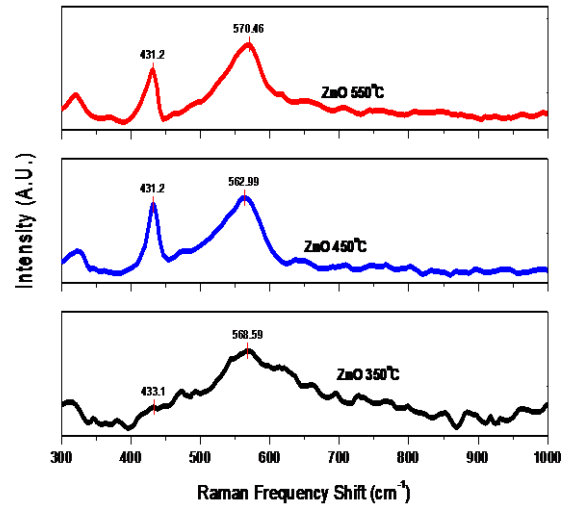
Figure 5 Raman peaks for ZnO at 350°C (a) 450°C (b) and 550°C (c)

C. UV-vis

The UV-vis measurements show the transmittance of ZnO-Graphene thin film that was prepared at 350°C-550°C ZnO growth temperature. The baseline for the measurement was Pt on glass substrate while the Pt/ZnO-Graphene thin film was measured against the baseline.

Figure 6 shows the transmittance of the Pt/ZnO-Graphene thin film on glass. The wavelength spectrum for the UV-vis measurement ranges from 300 nm to 800 nm. It can be seen that the transmittance of the samples ranges from 0 % at 300 nm to 92 % at 800 nm. At 550 nm wavelength, the transmittance for sample at 350°C, 450°C and 550°C is about 67.48 %, 64.69 % and 61.91 % respectively. The value is quite low because some of the residues from the graphene solution remain on the surface after the water bath. The residue hinders the light penetration as it is opaque in colour. On the other hand, thicker ZnO at high growth temperature has resulted in lower transmittance compared to low growth temperature.

The thickness in the sample can be attributed to the additional ZnO nanoparticles deposited on the sample during the cooling process of the TCVD. Longer time to cool at high temperature, namely 550˚C, may have caused further growth of the ZnO nanoparticles on the substrate, thus increasing the sample thickness.
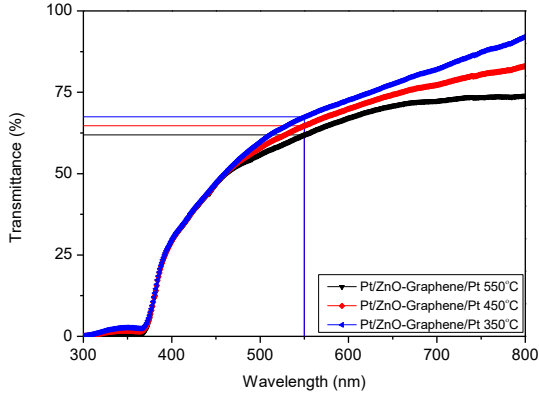
Figure 6 The UV-vis transmittance for ZnO samples prepared at 350˚C, 450˚C and 550˚C

D. I-V measurements

The two terminal I-V measurements were conducted by sweeping the applied DC voltage from 0V to 5V and from 0V to -5V. The TE is connected to the positive supply while the BE is connected to the negative supply. The stacking of Pt/ZnO/Pt and Pt/ZnO-Graphene/Pt follow the Metal-Insulator-Metal (MIM) configuration as shown in Figure 7. The resistance ratio Roff/Ron is calculated from the formula:

$$\frac{R_{off}}{R_{on}} = \frac{\frac{V_{off}}{I_{off}}}{\frac{V_{on}}{I_{on}}} = \frac{I_{on}}{I_{off}} \ since \ V_{off} = V_{on} \qquad (1)$$

where R_{off}, I_{off} and V_{off} are resistance, current and voltage during OFF mode respectively and R_{on}, I_{on} and V_{on} are resistance, current and voltage during ON mode respectively.

In Figure 8(a), the pinched hysteresis loop of the Pt/ZnO/Pt sample at 350˚C is large in quadrant 1 of the I-V plane but smaller in quadrant 3. The R_{off}/R_{on} ratio in quadrant 1 is about 3.17 and 1.65 in quadrant 3. The hysteresis window is also large on both sides for the Pt/ZnO/Pt sample prepared at 450˚C. The ratios of the sample in the 1st quadrant and 3rd quadrant are 1.90 and 3.00 respectively. The hysteresis window of the 550˚C Pt/ZnO/Pt sample is smallest compared to samples at lower temperature. The R_{off}/R_{on} ratio in the 1st quadrant is 2.61 while the 3rd quadrant is about 1.78. The R_{off}/R_{on} ratio of the samples with Graphene layer has shown a reduction. In Figure 8(b), the ratios of the Pt/ZnO-Graphene/Pt sample at 350˚C are 1.98 and 3.11 in quadrants 1 and 3 respectively. The ratios are 2.08 and 2.38 for the 450˚C sample while the ratios are 1.50 and 1.27 for the 550˚C sample respectively. The summary of the ratios is outlined in table 2.
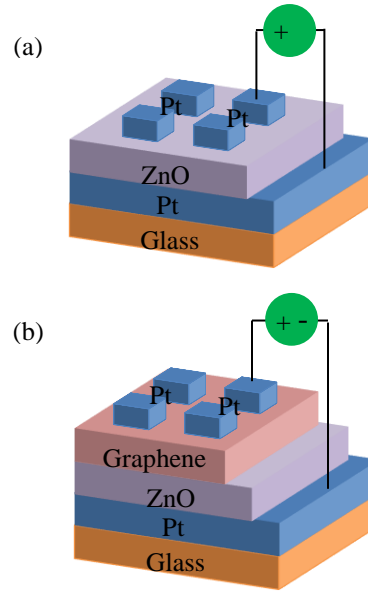
Figure 7 I-V measurement schematic illustration of the MIM configuration for (a) ZnO and (b) ZnO-Graphene samples
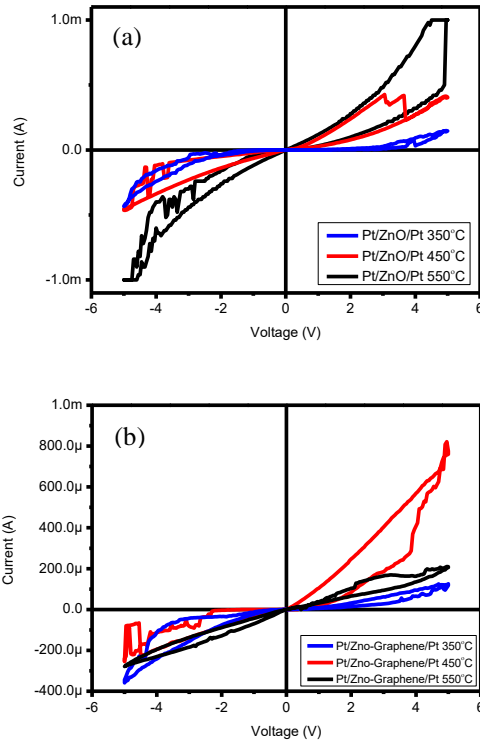
Figure 8 (a) shows the I-V measurements for ZnO samples and (b) shows the I-V measurements for ZnO-Graphene samples.

TABLE II.　　SUMMARY OF MEMRISTIVE EFFECTS

Device Structure	Growth temperature	Resistance Ratio 1st Quadrant	Resistance Ratio 3rd Quadrant	Resistive Switching Type
Pt/ZnO/Pt	350˚C	3.17	1.65	Bipolar
Pt/ZnO/Pt	450˚C	1.90	3.00	Bipolar
Pt/ZnO/Pt	550˚C	2.61	1.78	Bipolar
Pt/ZnO-Graphene/Pt	350˚C	1.98	3.11	Bipolar
Pt/ZnO-Graphene/Pt	450˚C	2.08	2.38	Bipolar
Pt/ZnO-Graphene/Pt	550˚C	1.50	1.27	Bipolar

The comparison of the ratio in both quadrants can be seen in Figure 9 where the I-V measurements are converted into semilogarithmic scale. From the comparison, the large hysteresis window can be attributed to the carrier concentration of oxygen vacancy [20]. More specifically, higher high resistance state (HRS) resistance is caused by the high oxygen vacancies while lower low resistance state (LRS) resistance is due to the improved crystallinity [21]. As seen in Figure 10, the change in the resistance from HRS to LRS is the largest in both 350˚C ZnO and hybrid samples. The HRS is 175 kΩ and LRS is 55 kΩ for the ZnO sample and 86.7 kΩ and 43.9 kΩ for the hybrid sample.

In the 350˚C ZnO and hybrid samples, the grain is small compared to the other samples, giving rise to the high occurrence of defects, namely oxygen vacancies [22]–[24]. As more oxygen vacancies are present, the formation of the conductive filament (CF) becomes faster, leading to high conductivity of the filament or in this case decreased LRS resistance. Therefore, the memristive window becomes larger than the other samples at 450˚C and 550˚C, whose grains are much bigger. However, lower HRS resistance in the 350˚C ZnO and hybrid samples can be attributed to the poor crystallinity of the samples as compared to the 450˚C and 550˚C ZnO and hybrid samples. Since the 450˚C and 550˚C ZnO and hybrid samples have larger grains and thicker films, evident in the FESEM and UV-vis results, their crystallinity is improved. As a result, the improved crystallinity in those samples has contributed to the high HRS resistance.
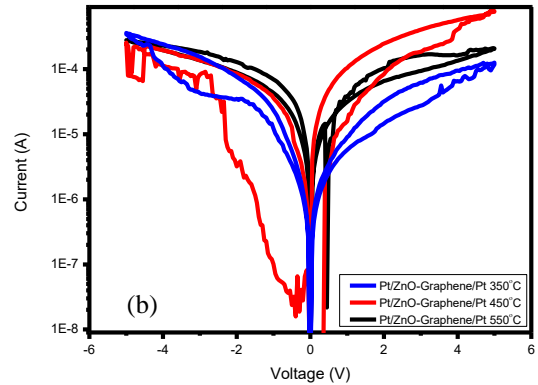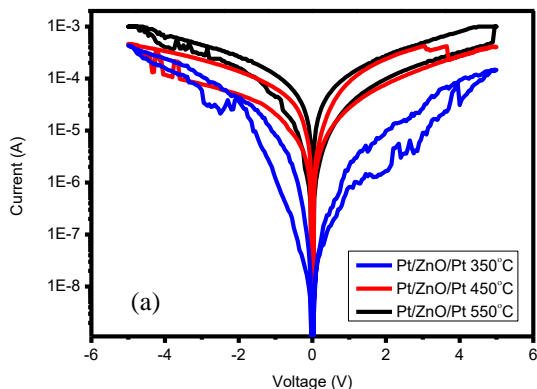
Figure 9 (a)-(b) Comparison of Roff/Ron of all samples in semilogarithmic scale
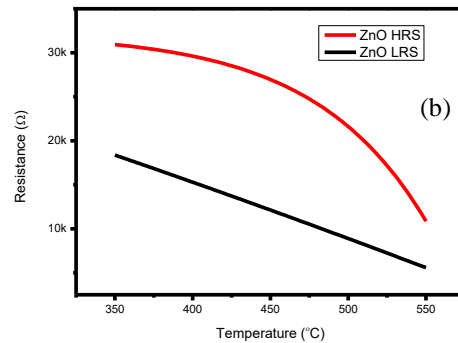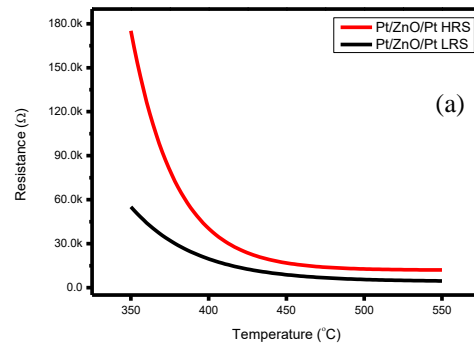
Figure 10 (a) HRS and LRS resistance for ZnO (b) ZnO-Graphene

Figure 11 and Figure 12 show the number of switching cycles for ZnO and ZnO-Graphene samples where the switching stability is increased when Graphene is added to the sample. In Figure 11, the hysteresis loop of ZnO samples is maintained at 4 cycles before it collapses. During the unstable cycle, the HRS and LRS merge, forming a very small resistance ratio. The sample cannot be switched ON and OFF because there is no discernible window that can define both states. On the other hand, the switching cycle of ZnO-Graphene in Figure 12 still maintains the memristive properties such as the resistance ratio at cycle 4. The HRS and LRS are well defined in both cycles 1 and 4. The memristive

effects are preserved with comparable resistance ratio throughout the cycles. This shows that the switching stability can be achieved in ZnO-Graphene samples, thus improving the uses of the samples in memory applications.
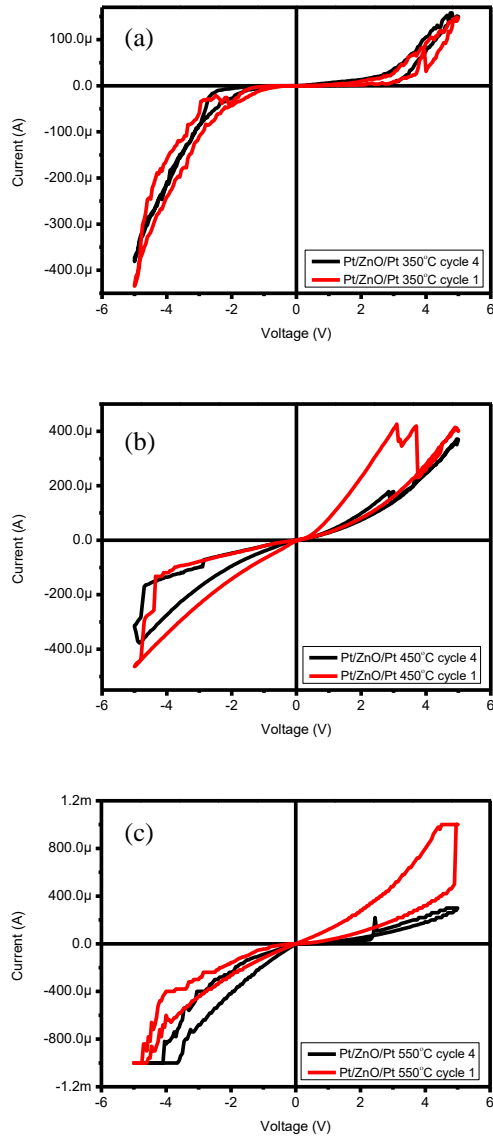
Figure 11 Number of cycles for Pt/ZnO/Pt samples
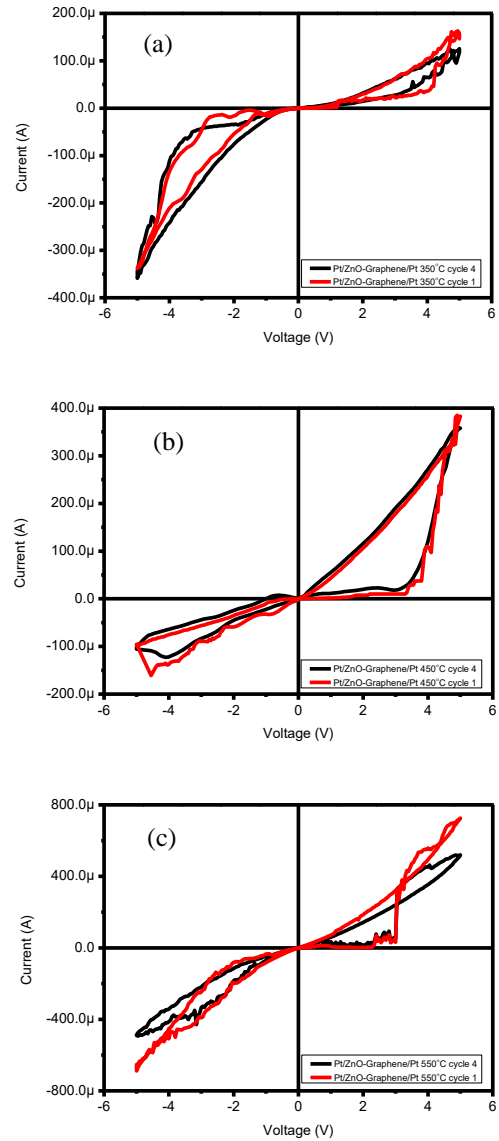
Figure 12 Number of cycles for Pt/ZnO-Graphene/Pt samples

E. Reliability of ZnO-Graphene devices

The reliability of the device is increased when Graphene is added to the ZnO thin film. From Figure 13, the number of cycles has increased to 17, 19 and 18 for 350˚C, 450˚C and 550˚C, respectively. In contrast, the cycle counts for the ZnO samples are much lower than the hybrid samples. This shows that the cycle stability is increased with the addition of Graphene, thus preserving the memristive properties of the samples and increasing the reliability of the devices.
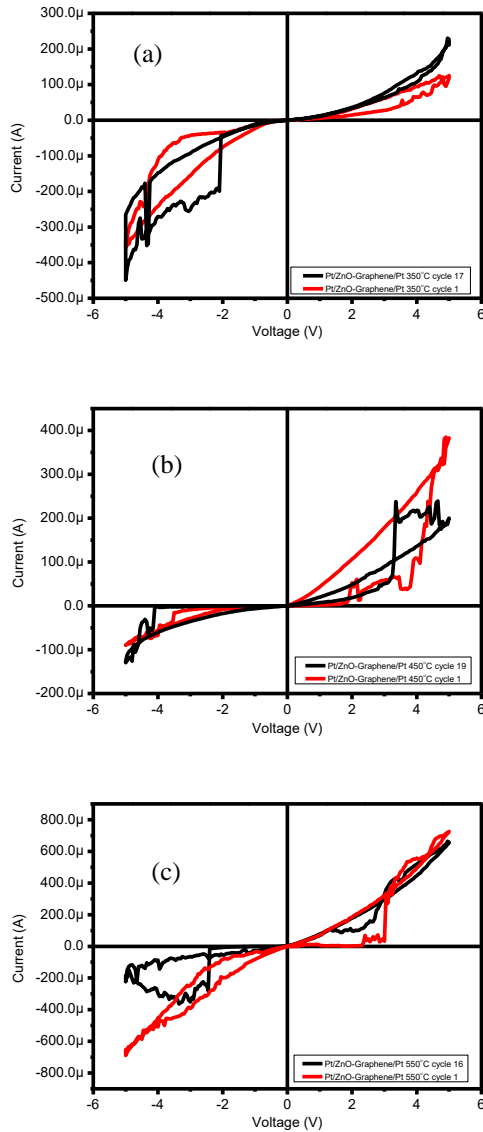
Figure 13 The extended number of cycles for Pt/ZnO-Graphene/Pt samples

IV. CONCLUSION

In summary, we fabricated two different devices, namely ZnO and ZnO-Graphene in order to investigate the effect of ZnO growth temperature on ZnO-Graphene devices. The ZnO-Graphene devices showed bipolar resistive switching characteristics with slightly smaller memristive window than those without Graphene. We found that ZnO prepared at 350˚C had the largest ratio for both ZnO and ZnO-Graphene devices. The grain structure of ZnO in the devices led to the changes in the oxygen vacancy concentration and the crystallinity. We also found that the addition of Graphene had improved the resistive switching stability.

REFERENCES

[1] S. Porro, E. Accornero, C. F. Pirri, and C. Ricciardi, "Memristive devices based on graphene oxide," *Carbon N. Y.*, vol. 85, no. January, pp. 383–396, 2015.

[2] K. Szot, W. Speier, G. Bihlmayer, and R. Waser, "Switching the electrical resistance of individual dislocations in single-crystalline SrTiO3," *Nat. Mater.*, vol. 5, no. 4, pp. 312–320, 2006.

[3] J. Wang, B. Sun, F. Gao, and N. C. Greenham, "Memristive devices based on solution-processed ZnO nanocrystals," *Phys. Status Solidi Appl. Mater. Sci.*, vol. 207, no. 2, pp. 484–487, 2010.

[4] K. M. Kim *et al.*, "Electrically configurable electroforming and bipolar resistive switching in Pt/TiO$_2$/Pt structures," *Nanotechnology*, vol. 21, no. 30, p. 305203, 2010.

[5] Y. Yang, S. Choi, and W. Lu, "Oxide heterostructure resistive memory," *Nano Lett.*, vol. 13, no. 6, pp. 2908–2915, 2013.

[6] Y. S. Kim *et al.*, "Resistive switching behaviors of NiO films with controlled number of conducting filaments," *Appl. Phys. Lett.*, vol. 98, no. 19, pp. 2009–2012, 2011.

[7] M. N. Kozicki and M. Mitkova, "Mass transport in chalcogenide electrolyte films - materials and applications," *J. Non. Cryst. Solids*, vol. 352, no. 6–7 SPEC. ISS., pp. 567–577, 2006.

[8] Y. Chen, G. Liu, C. Wang, W. Zhang, R.-W. Li, and L. Wang, "Polymer memristor for information storage and neuromorphic applications," *Mater. Horizons*, vol. 1, no. 5, p. 489, Jun. 2014.

[9] T. Berzina *et al.*, "Optimization of an organic memristor as an adaptive memory element," *J. Appl. Phys.*, vol. 105, no. 12, 2009.

[10] Y. Chen, B. Zhang, G. Liu, X. Zhuang, and E.-T. Kang, "Graphene and its derivatives: switching ON and OFF," *Chem. Soc. Rev.*, vol. 41, no. 13, p. 4688, 2012.

[11] F. Hui *et al.*, "Graphene and Related Materials for Resistive Random Access Memories," *Adv. Electron. Mater.*, vol. 1600195,

pp. 1–32, 2017.

[12]   J. Kim *et al.*, "Impact of graphene and single-layer BN insertion on bipolar resistive switching characteristics in tungsten oxide resistive memory," *Thin Solid Films*, vol. 589, pp. 188–193, 2015.

[13]   M. Qian *et al.*, "Tunable, Ultralow-Power Switching in Memristive Devices Enabled by a Heterogeneous Graphene-Oxide Interface," *Adv. Mater.*, vol. 26, no. 20, pp. 3275–3281, May 2014.

[14]   S. K. Min *et al.*, "Thickness Dependence of Properties of ZnO Thin Films on Porous Silicon Grown by Plasma-assisted Molecular Beam Epitaxy," *J. Korean Phys. Soc.*, vol. 59, no. 3, p. 2354, Sep. 2011.

[15]   S. H. Dalal, D. L. Baptista, K. B. K. Teo, R. G. Lacerda, D. a Jefferson, and W. I. Milne, "Controllable growth of vertically aligned zinc oxide nanowires using vapour deposition," *Nanotechnology*, vol. 17, no. 19, p. 4811, 2006.

[16]   I. R. M. Kottegoda *et al.*, "Comparison of Few-layer Graphene Prepared from Natural Graphite through Fast Synthesis Approach," *J. Mater. Sci. Technol.*, vol. 31, no. 9, pp. 907–912, 2015.

[17]   A. C. Ferrari and J. Robertson, "Interpretation of Raman spectra of disordered and amorphous carbon," *Phys. Rev. B*, vol. 61, no. 20, pp. 14095–14107, 2000.

[18]   J. Kim, S. N. F. Mohd Nasir, M. A. Mat Teridi, A. R. bin Mohd Yusoff, and J. Jang, "Zinc oxide nanorod doped graphene for high efficiency organic photovoltaic devices," *RSC Adv.*, vol. 6, no. 90, pp. 87319–87324, 2016.

[19]   G. Anoop, V. Panwar, T. Y. Kim, and J. Y. Jo, "Resistive Switching in ZnO Nanorods/Graphene Oxide Hybrid Multilayer Structures," *Adv. Electron. Mater.*, vol. 3, no. 5, p. 1600418, May 2017.

[20]   Y. Sun, X. Yan, X. Zheng, Y. Liu, Y. Shen, and Y. Zhang, "Influence of carrier concentration on the resistive switching characteristics of a ZnO-based memristor," *Nano Res.*, vol. 9, no. 4, pp. 1116–1124, 2016.

[21]   Y. Sun *et al.*, "High on-off ratio improvement of ZnO-based forming-free memristor by surface hydrogen annealing," *ACS Appl. Mater. Interfaces*, vol. 7, no. 13, pp. 7382–7388, 2015.

[22]   J. Iqbal, A. Jilani, P. M. Ziaul Hassan, S. Rafique, R. Jafer, and A. A. Alghamdi, "ALD grown nanostructured ZnO thin films: Effect of substrate temperature on thickness and energy band gap," *J. King Saud Univ. - Sci.*, vol. 28, no. 4, pp. 347–354, 2016.

[23]   S. Chen, N. Noor, I. P. Parkin, and R. Binions, "Temperature and thickness-dependent growth behaviour and opto-electronic properties of Ga-doped ZnO films prepared by aerosol-assisted chemical vapour deposition," *J. Mater. Chem. A*, vol. 2, no. 40, pp. 17174–17182, 2014.

[24]   E. Ş. Tüzemen, S. Eker, H. Kavak, and R. Esen, "Dependence of film thickness on the structural and optical properties of ZnO thin films," *Appl. Surf. Sci.*, vol. 255, no. 12, pp. 6195–6200, 2009.